VIRULENCE
2025, VOL. 16, NO. 1, 2551176
https://doi.org/10.1080/21505594.2025.2551176

Taylor & Francis
Taylor & Francis Group

BACTERIAL PATHOGENESIS

OPEN ACCESS Check for updates

Autophagy-driven modulation of stem cell dynamics in *Helicobacter pylori*-induced gastric diseases in mice

Jing Li*, Sisi Liu*, Zhiqin Li, Chunlei Ma, Boqing Li, Yingzi Cui, Wenke Wang, Huilin Zhao, Xiaofei Ji, and Ying Zhang

School of Basic Medical Sciences, Binzhou Medical University, Yantai, China

ABSTRACT

Chronic *Helicobacter pylori* infection is a major contributor to gastric disease progression, with its involvement in autophagy and stem cell dynamics playing a critical role in disease mechanisms. This study investigated how *H. pylori*, particularly in combination with the carcinogen N-nitroso-N-methylurea (NMU), disrupted autophagy and stem cell function, driving gastric pathology. *H. pylori* infection significantly increased autophagy, promoted the epithelial–mesenchymal transition, suppressed *Tff2* and *Ghrelin* expression in mouse gastric organoids, and enhanced stem cell proliferation (organoid numbers increased 92% compared to control at 24 weeks, $p < 0.001$), while NMU caused milder autophagy, severe inflammation, glandular dilation, and reduced stemness markers (CD133 decreased 30% at 24 weeks, $p < 0.05$). Combined *H. pylori* and NMU exposure synergistically dysregulated *Tff2*/*Ghrelin* expression, exacerbated autophagic flux disruption, and impaired stem cell function, reducing organoid budding (decreased 43% vs. *H. pylori* alone at 36 weeks, $p < 0.01$) and dysregulating *CD133*, *CD44*, *Lgr5*, and *SOX2* expression. Pathologically, this combination led to severe gastric damage, including intestinal metaplasia and neutrophil infiltration. Chloroquine (CQ) treatment mitigates these effects by reversing autophagic dysfunction, restoring stem cell capacity (*Lgr5* increased 97% at 44 weeks, $p < 0.05$), differentially modulating *Tff2*/*Ghrelin*: potentiating *Tff2* and suppressing Ghrelin, normalizing organoid growth, attenuating the EMT, and reducing inflammation, particularly in the *H. pylori* + NMU group. These findings elucidate how *H. pylori* and NMU drive gastric pathology through autophagy-stem cell crosstalk and highlight CQ's potential as a targeted therapeutic strategy for infection-associated gastric damage.

ARTICLE HISTORY
Received 27 January 2025
Revised 16 July 2025
Accepted 14 August 2025

KEYWORDS
Helicobacter pylori; autophagy; epithelial-mesenchymal transition (EMT); organoid; chloroquine; N-nitroso-N-methylurea (NMU)

Introduction

Gastric diseases, including gastritis and gastric cancer, are strongly associated with *Helicobacter pylori* infection, which affects a substantial portion of the global population [1,2]. *H. pylori* infection is a key driver of various gastric conditions, ranging from inflammation and ulcers to more severe outcomes such as cancer. This disease is multifactorial, progressing through a complex, prolonged course influenced by various environmental, genetic, and microbial factors [3]. The pathogenicity of *H. pylori* involves its ability to deliver virulence factors into host cells, disrupting normal cellular processes, and leading to tissue damage [4,5]. This disruption can cause abnormal stem cell behavior, contributing to both precancerous conditions and cancer development [6,7]. *H. pylori* alter stem cell dynamics by inducing uncontrolled proliferation and survival of these cells, laying the foundation for precancerous changes that can lead to the development of gastric cancer [8].

Stem cells play a critical role in maintaining gastric tissue homeostasis through self-renewal and differentiation [9]. Under normal conditions, these processes are tightly regulated, but *H. pylori* infection can disrupt this balance, leading to altered stem cell dynamics and disease progression [8]. One key factor in this process is autophagy, a cellular degradation pathway that helps regulate stem cell function, tissue repair, and responses to infection [10].

Autophagy influences gastric stem cell behavior by regulating cellular homeostasis and stress responses, contributing to both inflammation and oncogenesis [11,12]. Notably, autophagy interacts with the epithelial – mesenchymal transition (EMT). The EMT enhances cell migration, invasion, and stemness acquisition [13,14], and its crosstalk with autophagy drives tissue pathology through pathways like PI3K/AKT/mTOR, AMPK, and TGF-β [15]. PI3K/AKT/mTOR hyperactivation suppresses epithelial markers and upregulates mesenchymal markers via Twist/Snail/ZEB1,

CONTACT Ying Zhang zhangying@bzmc.edu.cn; Boqing Li liboqing@bzmc.edu.cn
*These authors contributed equally to the paper.
Supplemental data for this article can be accessed online at https://doi.org/10.1080/21505594.2025.2551176.

while its inhibition reverses these effects [16]. AMPK, activated by LKB1 or ghrelin, inhibits mTOR to promote autophagy and suppresses the EMT by targeting Snail and Hedgehog/Gli1 [17]. TGF-β drives the EMT via SMAD/non-SMAD pathways and induces autophagy through BECN1/ATG5/ATG7, with context-dependent outcomes [18]. Notably, these pathways are co-opted during *H. pylori* infection, where chronic inflammation disrupts the autophagy – EMT balance. The loss of epithelial markers (e.g. E-cadherin) and gain of mesenchymal markers (e.g. α-SMA, vimentin) not only facilitate the EMT but also alter stem cell plasticity, promoting gastritis-to-cancer transition [19,20]. This synergy between autophagy dysregulation and EMT activation not only remodels gastric epithelium but also accelerates the Correa cascade, highlighting their dual role as therapeutic targets in *H. pylori*-associated carcinogenesis.

Organoids, which are three-dimensional structures derived from stem cells, have emerged as a powerful tool for studying tissue biology. Organoids replicate the structure and function of real organs, providing an advanced platform for studies [21]. In 2009, small intestinal organoids from $Lgr5^{+}$ stem cells in mice were successfully cultured, demonstrating the potential of organoid technology in research [22]. Based on past studies, the size, number, and budding of organoids serve as important indicators of stem cell dynamics, including their capacities for proliferation, differentiation, and self-renewal, as reported in numerous studies [23–25]. These morphological features reflect the functional state of stem cells and also provide a model for understanding developmental processes and tissue regeneration, highlighting their relevance in modeling organogenesis and disease. While most studies on *H. pylori* -related gastric diseases still rely on traditional two-dimensional cell cultures and mouse models [26], organoids provide a more physiologically relevant system for studying how *H. pylori* affect stem cell dynamics during the progression of gastric diseases.

In recent decades, the link between *H. pylori* infection and the progression of gastric diseases, such as gastritis and gastric cancer [27], has been well-established. However, despite extensive research, the interactions between *H. pylori*, host cell autophagy, and stem cell dynamics remain only partially understood, particularly in the presence of exposure to carcinogens, which significantly alters the gastric tissue microenvironment. N-nitroso-N-methylurea (NMU), a potent alkylating agent, induces gastric epithelial DNA damage and synergizes with *H. pylori*-induced inflammation to model early-stage gastric pathology [28,29]. This study therefore aimed to: (1) clarify how *H. pylori* and NMU exposure enhances autophagic activity; (2) reveal how autophagy dysregulation influences the EMT and disrupts stem cell function; and (3) investigate how chloroquine (CQ), an autophagy inhibitor, mitigates pathological changes by restoring normal stem cell function and promoting tissue repair. These findings provide new insights into potential therapeutic approaches for *H. pylori*-related gastric diseases and emphasize the importance of targeting autophagy as a novel strategy for various treatments.

Materials and methods

Bacterial culture

The SS1 strain of *Helicobacter pylori*, stored as a glycerol stock at – 80°C in the Pathogenic Biology Laboratory of Binzhou Medical University, was revived by thawing at room temperature and washing in sterile phosphate-buffered saline (PBS). The revived strain was inoculated by streaking approximately 100 μL of bacterial suspension onto Karmali agar plates (OXOID, CM0935, GBR), which contained 39.0 g/L Columbia agar base, 4.0 g/L activated charcoal, and 32 mg/L hemin chloride, adjusted to pH 7.2 ± 0.2 (at 25°C post-sterilization), and supplemented with 5% defibrinated sheep blood. Plates were incubated at 37°C in a three-gas incubator (Thermo, 3131, USA) under microaerophilic conditions (5% O_2, 10% CO_2, 85% N_2). Bacterial growth was monitored every 2–3 d, and fresh Kamali agar plates were prepared as needed to maintain optimal growth conditions.

Animal model establishment and sampling

For this study, 5-week-old male C57BL/6 mice were sourced from Jinan Pengyue Experimental Animal Breeding Co., Ltd. (SCXK Lu 20,190,003, China) and kept in specific pathogen-free facilities with a 12-hour light/dark cycle, at 22 ± 1°C and 40–60% humidity. After 1 week of adaptation, the mice were randomly divided into four groups: Control, *H. pylori*, NMU, and *H. pylori* + NMU ($n = 45$ per group). The initial grouping of mice was performed using a random number table to ensure unbiased allocation. An independent researcher, who was not involved in subsequent experimental procedures, assigned each mouse a unique identifier and allocated them to groups according to the pre-generated random sequence. The Control group received no treatment, while the *H. pylori* group was administered *H. pylori* (SS1 strain) by gastric gavage (0.6 mL of bacterial suspension at 1×10^9 cfu/mL) every other day for 3 weeks. The NMU group was gavaged

with NMU (5 mg/3 mL, 0.3 mL) weekly for 10 weeks. The *H. pylori* + NMU group received *H. pylori* for 3 weeks, followed by NMU for 10 weeks. The control group was maintained under identical baseline conditions to the experimental groups, providing reference values for normal physiological parameters throughout the study period. The single-treatment groups (*H. pylori*-only and NMU-only groups) were designed to assess the individual effects of each intervention, whereas the combined treatment group (*H. pylori* + NMU) allowed evaluation of potential synergistic effects between the two agents.

At 41 weeks of age, mice were further divided into two subgroups: one group receiving phosphate-buffered saline (PBS) gavage (0.5 mL) and the other receiving intraperitoneal injections of CQ (60 mg/kg, 0.5 mL) daily for 1 week. This resulted in eight groups: Control, *H. pylori*, NMU, *H. pylori* + NMU, Control + CQ, *H. pylori* + CQ, NMU + CQ, and *H. pylori* + NMU + CQ. The position of each mouse cage was re-shuffled at the end of intragastric treatment to ensure that there was no fixed order of treatment. Each time, the numbers were re-arranged and processed in a randomly generated sequence to ensure treatment randomization. Intraperitoneal injection was performed in a similar manner. All mouse treatments were performed by two separate individuals, and no specific grouping was given. The weight and hair status of the animals were observed every week. From the end of drug treatment to the end of the experiment, the mice had normal food and water intake, normal hair, and slightly decreased weight; quality of life of the mice was ensured as best as possible.

Mice were euthanized at 24, 36, and 44 weeks of age, and gastric tissues were collected for analysis. At 24 weeks of age, gastric tissues were collected to confirm successful colonization of *H. pylori* using Giemsa staining. To confirm *H. pylori* colonization and exclude contamination, gastric tissue samples were subjected to PCR amplification of the pathogen-specific *cytotoxin-associated gene A* (*cagA*) gene, a standard virulence marker for *H. pylori* identification. Gastric tissues were collected at 24, 36, and 44 weeks for hematoxylin and eosin staining, and immunohistochemistry analyses for E-cadherin and vimentin. Stem cells were isolated for organoid culture. Subsequently, the development and differentiation of the organoids were examined. At 24 and 44 weeks, LC3B (microtubule-associated protein 1A/1B-light chain 3B) levels were assessed by immunohistochemistry and autophagosomes/autolysosomes were analyzed by transmission electron microscopy (TEM). For each independent experiment, six samples of stomach tissue were selected from six random mice in each group. No animals died during the experiment.

The study was approved by the Animal Use and Care Committee of Binzhou Medical University (Approval No. 2021–012), with all procedures complying with national and international standards for animal care and use. The ethical review process entails a thorough assessment of the experimental protocol, animal welfare provisions, and study endpoints to ensure adherence to institutional and regulatory ethical standards. All procedures were performed in accordance with ARRIVE 2.0 guidelines, with particular attention to randomization, blinding and sample size calculation to ensure robust and unbiased experimental design. A completed ARRIVE checklist has been provided as supplementary material.

Giemsa staining

Gastric tissues were dissected, and paraffin sections were prepared. Giemsa staining solution was made by diluting concentrated Giemsa solution 1:9. Fresh Giemsa dye solution was prepared, and paraffin was removed with xylene followed by dehydration with gradients of alcohol. The dye was applied to the slides, covering all specimens, and stained for 20 minutes. After rinsing with tap water, the samples were cleared with gradient alcohol and xylene, sealed with neutral gum, and observed under a light microscope for imaging.

DNA extraction and cagA gene amplification

Genomic DNA from mouse tissues was extracted using a Tiangen Genomic DNA Extraction Kit (DP304, CHN) according to the manufacturer's instructions. DNA was extracted from 0.01 g of gastric tissue collected from 5-week-old C57BL/6 mice. The tissue was chopped, suspended in 1 mL of PBS, homogenized using ultrasound, and centrifuged. The resulting pellet was resuspended in 200 µL of buffer GA, followed by the addition of 4 µL of RNase A, and incubated at room temperature for 5 minutes. Then, 20 µL of proteinase K was added and the mixture was incubated at 56°C for 1 hour. The solution was then treated with buffer GB and ethanol, purified using a spin column, and DNA was isolated for subsequent PCR analysis.

The *H. pylori cagA* gene was amplified using primers *cagA*-F and *cagA*-R (Table 1) designed from the SS1 strain sequence. The 25 µL PCR reaction consisted of 12.5 µL mix, 1 µL of each primer, 1 µL template DNA, and 9.5 µL nuclease-free water. The amplification was conducted under the following conditions: initial

Table 1. Primers used in this study.

Primer name	Primer Sequence
cagA-F	5″-GAGCCTACTGGTGGGGATTG-3″
cagA-R	5″-TGTGAGCCTGTGAGTTGGTC-3″
GAPDH-F	5″-AGTATGACTCCACTCACGGCAA-3″
GAPDH-R	5″-ACACCAGTAGACTCCACGACA-3″
E-cadherin-F	5″-GATCCTGACCAGCAGTTCGTT-3″
E-cadherin-R	5″-GGGCTTCATTCACGTCTACCAC-3″
Tff2-F	5″-TCCAAACCAAGAATCGGAGCAG-3″
Tff2-R	5″-ACCCACAATTCTTGCGAGCTGA-3″
Ghrelin-F	5″-ATGCTGTCTTCAGGCACCATC-3″
Ghrelin-R	5″-CTCCTGACAGCTTGATGCCAAC-3″
CD133-F	5″-CTGGTGGGCTGCTTCTTTTGTATG-3″
CD133-R	5″-CCGAGTCCTGGTCTGCTGGTTAG-3″
CD44-F	5″-CACATATTGCTTCAATGCCTCAG-3″
CD44-R	5″-CCATCACGGTTGACAATAGTTATG-3″
Lgr5-F	5″-GACAATGCTCTCACAGAC-3″
Lgr5-R	5″-GGAGTGGATTCTATTATTATGG-3″
SOX2-F	5″-GCACATGAACGGCTGGAGCAACG-3″
SOX2-R	5″-TGCTGCGAGTAGGACATGCTGTAGG-3″

denaturation at 95°C for 30 seconds, followed by 40 cycles of 95°C for 30 seconds, 60°C for 30 seconds, and 72°C for 1 minute, with a final extension at 72°C for 10 minutes. The PCR products were verified using agarose gel electrophoresis.

Immunohistochemical staining

Paraffin-embedded sections of mouse gastric tissue were prepared for immunohistochemistry. Sections were dried at 60°C for 2 hours, dewaxed, and rehydrated. Following antigen retrieval and peroxidase inactivation, sections were blocked with serum for 15 minutes. Primary antibodies were incubated overnight at 4°C. Secondary antibody (goat anti-mouse/rabbit IgG polymer; Cell Signaling Technology, USA) was then applied and incubated at 37°C for 30 minutes. DAB (3,3'–diaminobenzidine) solution was used for visualization, with staining observed under a light microscope for 1–5 minutes. Hematoxylin counterstaining was performed for 2 minutes, followed by treatment with 1% hydrochloric acid/alcohol for 5 seconds. The sections were then rinsed, dehydrated, cleared, and mounted with neutral gum. Under the microscope, nuclei were stained blue-purple and positive regions appeared yellow-brown.

Transmission electron microscopy (TEM)

Mouse gastric tissues were dissected and fixed in 4% paraformaldehyde for 20 minutes followed by treatment with 2.5% glutaraldehyde at 4°C for 2 hours. Tissues were washed in 0.1 M PBS, then fixed in 1% osmium tetroxide at 4°C for 90 minutes. After washing, the tissues were dehydrated using graded ethanol (50%, 70%, 80%, 95%, and 100%) and acetone. Tissues were then impregnated with acetone-to-embedding reagent mixtures at ratios of 2:1, then 1:2 at 37°C. Polymerization was conducted by embedding the tissues in resin at 60°C for 48 hours. Ultrathin sections (70 nm) were cut, placed on copper grids, and stained with 2% uranyl acetate for 15 minutes and lead citrate for 5 minutes. After washing and drying, sections were examined using a transmission electron microscope (Hitachi, HT-7800, Japan).

Gastric organoid culture

The gastric organoid culture protocol was established based on modified methods from Sato et al. [22] and Sato & Clevers [25]. C57BL/6 mice were euthanized by cervical dislocation following intraperitoneal anesthesia, then sterilized by immersion in 75% alcohol. The stomach was aseptically dissected on a sterile surface maintained on crushed ice, and the luminal contents were thoroughly rinsed with ice-cold Dulbecco's phosphate buffered saline (DPBS). The tissue was then transferred to a sterile 10 cm^2 Petri dish and washed three times with chilled DPBS to remove residual debris. Under sterile conditions, the cleaned gastric tissue was minced into 1–2 mm^3 fragments using sterile surgical blades. The pieces were transferred to a centrifuge tube, washed with DPBS by gentle pipetting, and the supernatant was replaced repeatedly until it became clear. The tissue fragments were enzymatically digested at 37°C for 1 hour in a digestion solution containing collagenase IV (1 mg/mL), hyaluronidase (0.5 mg/mL), 20% fetal bovine serum (FBS), and 1% penicillin-streptomycin (P/S) in RPMI-1640 base medium (total volume of 10 mL). The reaction was terminated by adding an equal volume of fresh RPMI-1640 medium. The suspension was filtered twice through a 200-mesh cell strainer to obtain a single-cell suspension, which was centrifuged at 500 × *g* for 10 minutes at 4°C. The resulting pellet was resuspended in 1640 medium as required for the experiment. The single-cell suspension was mixed 1:1 with Matrigel, seeded at 50 µL per well in a preheated 24-well plate, and incubated at 37°C for 30 minutes to facilitate formation of a solid. Organoid medium was subsequently added and the cells were cultured at 37°C in a 5% CO_2 incubator with medium changes every 2 d. Organoid growth was monitored using a light microscope.

Real-time quantitative PCR (qPCR)

Approximately 0.01 g of gastric tissue was homogenized in 1 mL of TRIzol reagent (Invitrogen , USA) and incubated on ice for 30 minutes. After adding 200 µL of chloroform, the mixture was shaken for 30 seconds, left on ice for 3 minutes, and centrifuged at 12,000 × *g* for 15 minutes at 4°C. The supernatant was mixed with an equal volume of isopropanol, then incubated at room temperature for 20

minutes before repeating centrifugation. The resulting RNA pellet was washed with 75% ethanol, air-dried, and dissolved in 20 μL enzyme-free water. For reverse transcription yielding cDNA, 8 μL RNA was mixed with 2 μL enzyme (SparkJade, AG0304, CHN) and incubated at 42°C for 5 minutes, followed by incubation at 85°C for 5 minutes. The qPCR reaction mix contained 2.0 μL cDNA, 0.4 μL SYBR Green Master Mix (ROX) (SparkJade, AH0104, CHN), 0.4 μL of forward and reverse primers (Table 1), and 6.8 μL nuclease-free water, making a total volume of 10 μL per reaction. The qPCR was performed using a thermal cycler (Thermo Fisher Scientific, USA) with the following program: 50°C for 2 minutes, 95°C for 30 seconds, followed by 40 cycles of 95°C for 5 seconds, and 60°C for 30 seconds. The number of cycle values were recorded and relative gene expression was calculated using GAPDH as the internal reference.

Haematoxylin and eosin (H&E) staining

Gastric tissues were washed, sectioned, and fixed in 4% paraformaldehyde for 24 hours. After rinsing in PBS, the tissues underwent dehydration with graded concentrations of ethanol (75% for 5 minutes, 85% for 5 minutes, and 95% twice for 15 minutes), followed by paraffin embedding and sectioning. Slides were dried and baked at 60°C for 2 hours before dewaxing and hematoxylin staining for 8 minutes. Differentiation was conducted with 1% hydrochloric acid/alcohol for 30 seconds, followed by rinsing, eosin staining for 5 minutes, and dehydration using anhydrous ethanol. After clearing with xylene, the slides were sealed with neutral gum and viewed using a light microscope.

Statistical analysis

Quantitative data were expressed as means ± standard deviation (SD) and analyzed using one-way analysis of variance (ANOVA) in SPSS Statistics (version 22.0), and group differences were compared using Bonferroni's post hoc test. Statistical charts were created with GraphPad Prism and Adobe Illustrator. Statistical significance was defined as follows: $^{*}p < 0.05$, $^{**}p < 0.01$, $^{***}p < 0.001$, and $^{****}p < 0.0001$.

Results

H. pylori chronic infection induces autophagy dysregulation in gastric tissue

Giemsa staining confirmed the presence of *H. pylori* in the gastric tissue of infected mice, revealing its characteristic slender, curved, rod-shaped morphology. PCR amplification further identified the *H. pylori cagA* gene, and sequencing confirmed the gene sequence. These results demonstrated successful establishment of the *H. pylori*-infected mouse model (Figure S1).

To investigate the role of autophagy in gastric tissue during chronic *H. pylori* infection, immunohistochemical staining for LC3B was performed (Figure 1A). LC3B expression in 24-week-old mice was higher in the *H. pylori* group compared with the control group, and the *H. pylori* + NMU group showed elevated LC3B levels compared with the NMU group. In 44-week-old mice (Figure 1B), LC3B expression remained higher in the *H. pylori* group than that in the control group, and the *H. pylori* + NMU group continued to show higher LC3B expression than the NMU group. After CQ treatment, autophagy was inhibited, leading to the accumulation of LC3B. Expression of LC3B was higher in the *H. pylori* + CQ group compared with the *H. pylori* group, and the *H. pylori* + NMU + CQ group showed increased LC3B levels relative to the *H. pylori* + NMU group.

To assess the effects of autophagy at the ultrastructural level, TEM was performed. In 24-week-old mice (Figure 2A), the *H. pylori* group showed more pronounced mitochondrial ridge dissolution compared with the NMU group. Ribosome adhesion was observed on the rough endoplasmic reticulum (ER) and cytoplasmic surfaces, with enlarged cisternal spaces and moderate ER expansion accompanied by membrane dissolution. Autophagic lysosomes, enclosed by a single membrane, were also present. In the *H. pylori* + NMU group, ER and cisternal spaces were significantly enlarged, with marked degranulation of cytoplasmic ribosomes. Autophagic lysosomes were observed, indicating more severe autophagy compared with the *H. pylori* group.

In 44-week-old mice (Figure 2B), extensive autophagic lysosomes, coated with a single membrane, were observed in both the *H. pylori* and *H. pylori* + NMU groups. These lysosomes contained dissolved cell contents, and the myeloid forms represented the final stage of autophagic hydrolysis. No significant autophagy was seen in the NMU group. After CQ treatment, autolysosome degradation was inhibited, leading to the accumulation of single-membrane autolysosomes with dissolved contents. The *H. pylori* + CQ group exhibited an increased number of autophagic lysosomes and significant ER dilation with membrane dissolution. Similarly, in the *H. pylori* + NMU + CQ group, the number of autophagic lysosomes and smooth ER expansion further increased.

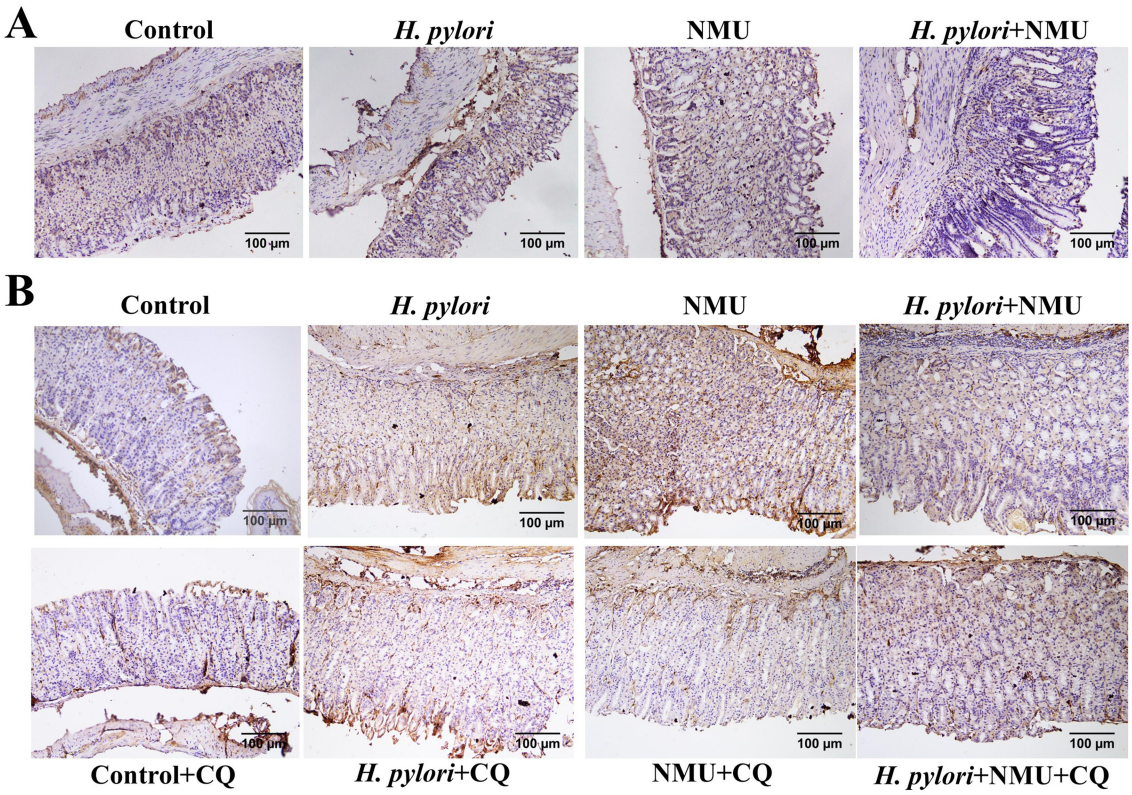

Figure 1. LC3B accumulation in gastric tissues during chronic *H. pylori* infection, N-nitroso-N-methylurea (NMU) treatment, and chloroquine (CQ) treatment. (A) immunohistochemical staining for LC3B in gastric tissues of 24-week-old mice across experimental groups: control, *H. pylori*, NMU, *H. pylori* + NMU ($n = 6$). (B) LC3B expression were observed in 44-week-old mice across experimental groups: control, *H. pylori*, NMU, *H. pylori* + NMU, *H. pylori* + CQ, and *H. pylori* + NMU + CQ ($n = 6$). Scale bar: 100 μm.

CQ treatment attenuates H. pylori- and NMU-mediated EMT

At both 24 and 36 weeks of age, immunohistochemistry staining revealed a consistent reduction in the epithelial marker E-cadherin in the *H. pylori* and *H. pylori* + NMU groups, when compared with the control and NMU groups. Furthermore, the mesenchymal marker vimentin was significantly elevated in the *H. pylori* and *H. pylori* + NMU groups, indicating EMT progression. These changes suggested that *H. pylori* infection, especially in combination with NMU, promoted the EMT, leading to alterations in gastric tissue structure (Figure 3A,B). At later stages of the experiment, the EMT became even more pronounced, with further decreases in E-cadherin and increased vimentin levels in the *H. pylori* and *H. pylori* + NMU groups. However, after CQ treatment, the EMT was partially reversed, as shown by higher E-cadherin and lower vimentin expressions in the *H. pylori* + CQ and *H. pylori* + NMU + CQ groups, suggesting an improvement in the EMT (Figure 3C).

Changes in E-cadherin, Tff2, and ghrelin expression during gastric organoid development

Expression of *E-cadherin*, *Tff2*, and *Ghrelin* during gastric organoid development was examined under different treatment conditions (Figure 4). Compared to controls, *H. pylori* infection led to a progressive decrease in *E-cadherin* levels at all time points: 0.71-fold at 24 weeks, 0.64-fold at 36 weeks, and 0.62-fold at 44 weeks. The combination of *H. pylori* and NMU further reduced *E-cadherin* at 24 weeks. However, treatment with CQ restored *E-cadherin* expression, with the *H. pylori* + CQ group reaching 2.35-fold and the *H. pylori* + NMU + CQ group showing a 1.62-fold increase, consistent with immunohistochemical findings.

To investigate the link between *H. pylori*-induced autophagy and the EMT, *Tff2*, and *Ghrelin* expression was quantified: At 24 weeks, *H. pylori* significantly suppressed both genes versus controls. The *H. pylori* + NMU group showed further reductions compared to NMU alone ($\Delta Tff2$: −25%; $\Delta Ghrelin$: −36%; $p < 0.01$). By 36 weeks, *H. pylori* infection induced divergent effects: *Tff2* became elevated, while *Ghrelin* remained

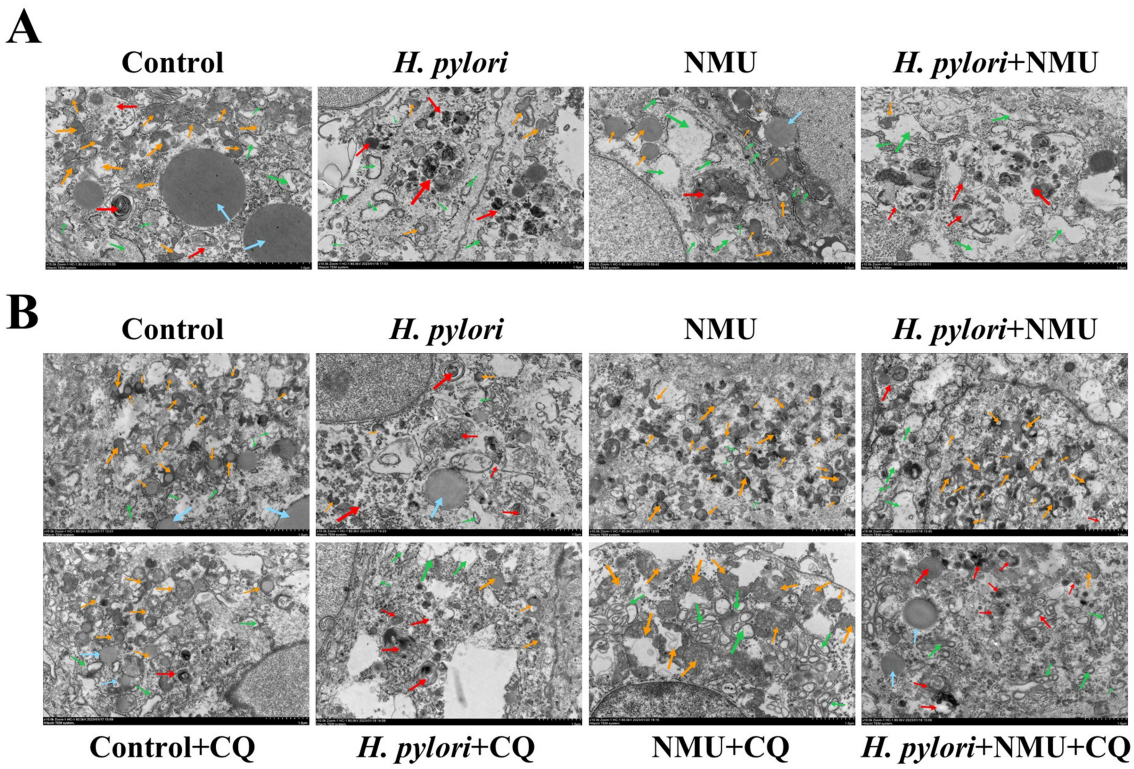

Figure 2. Accumulation of autophagosomes and autolysosomes in gastric tissues of mice exposed to *H. pylori*, N-nitroso-N-methylurea (NMU), and chloroquine. (A) transmission electron microscopy of autophagy-related structures in gastric tissue of 24-week-old mice: control group, *H. pylori* group, NMU group, *H. pylori* + NMU group ($n = 5$ independent fields of view analyzed per group). (B) autophagy-related structures were observed in the stomach tissue of 44-week-old mice under transmission electron microscopy across the following groups: control, *H. pylori*, NMU, and *H. pylori* + NMU. Orange arrows, mitochondria; green arrows, rough endoplasmic reticulum; blue arrows, free lipid droplets; and red arrows, polyvesicular bodies and medullary structures ($n = 5$ independent fields of view analyzed per group).

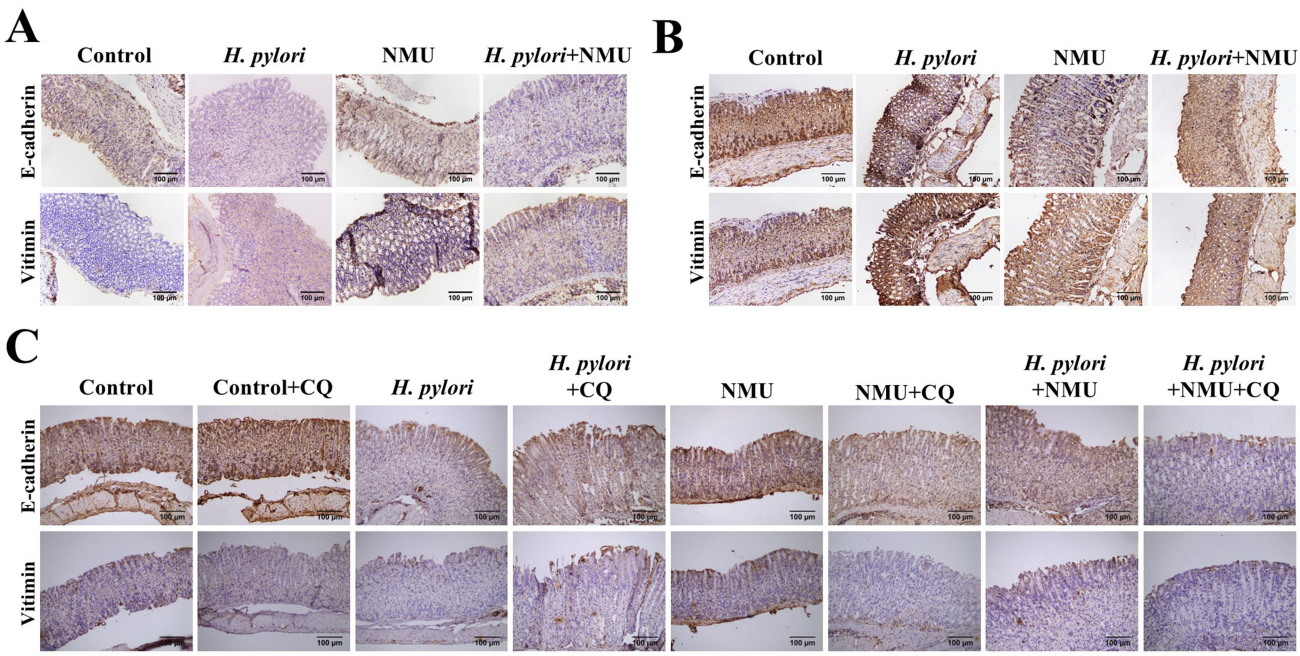

Figure 3. Epithelial–mesenchymal transition (EMT) in gastric tissues of mice under *H. pylori*, N-nitroso-N-methylurea (NMU), and chloroquine (CQ) exposure. (A, B) immunohistochemical staining for E-cadherin and vimentin at 24 and 36 weeks across experimental groups: control, *H. pylori*, NMU, *H. pylori* + NMU ($n = 6$). (C) immunohistochemical staining for E-cadherin and vimentin at 44 weeks across experimental groups: control, *H. pylori*, NMU, *H. pylori* + NMU, *H. pylori* + CQ, and *H. pylori* + NMU + CQ. Scale bar: 100 μm.

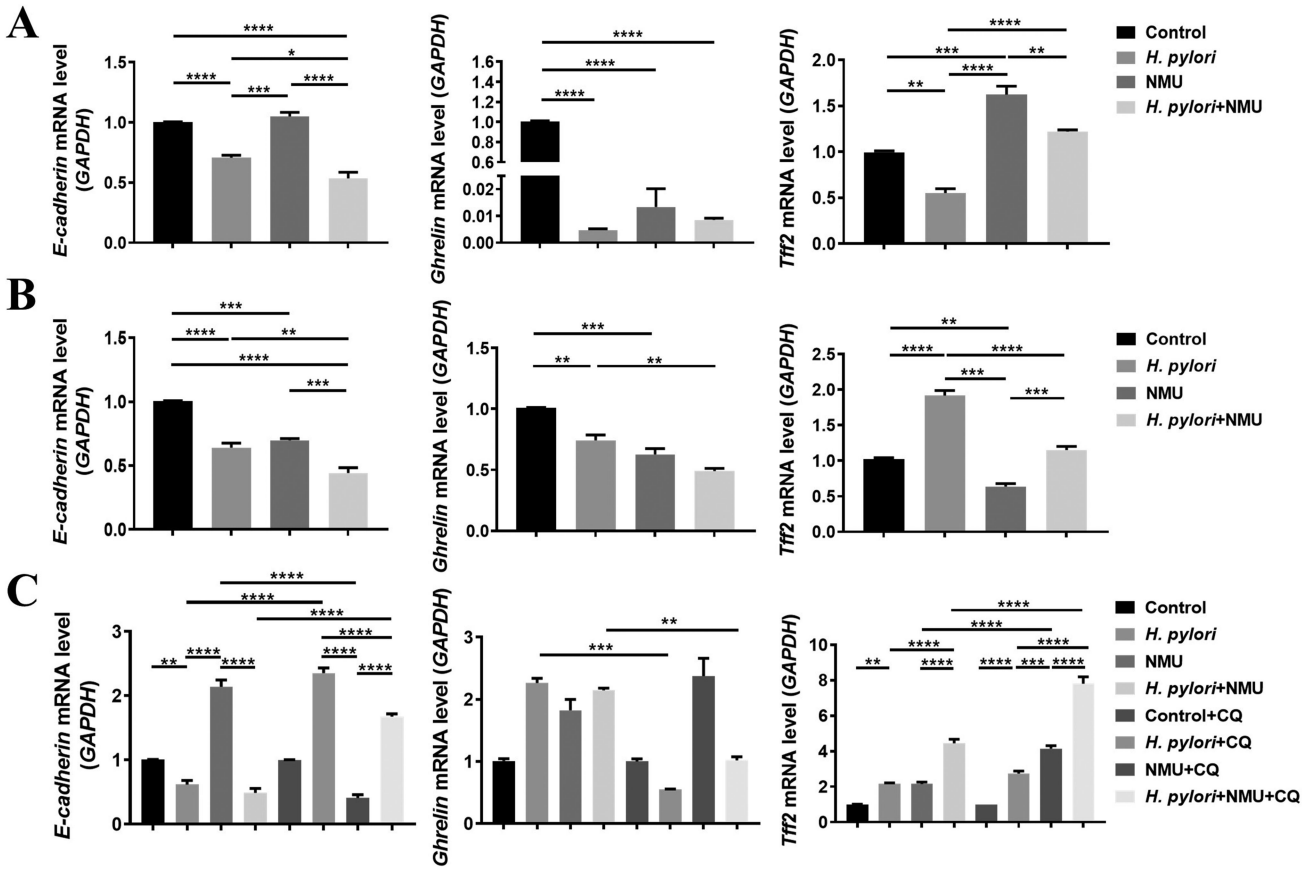

Figure 4. *E-cadherin*, *Ghrelin*, and *Tff2* expression profiles in mouse gastric organoid. Quantitative PCR analysis of *E-cadherin*, *Ghrelin*, and *Tff2* mRNA expression levels in gastric organoids from mice at (A) 24, (B) 36, and (C) 44 weeks post-treatment ($n = 3$). Statistical significance: *$p < 0.05$, **$p < 0.01$, ***$P < 0.001$, ****$p < 0.0001$.

suppressed. The *H. pylori* + NMU group exhibited synergistic upregulation of *Tff2*. At 44 weeks, all treatment groups showed marked *Tff2* upregulation (*H. pylori*: 2.18-fold; NMU: 2.15-fold; $p < 0.01$ vs. control). CQ treatment differentially modulated this response, potentiating *Tff2* in the *H. pylori* + NMU + CQ group but suppressing *Ghrelin*.

H. pylori and NMU alter gastric organoid morphology and budding capacity

To evaluate the proliferative capacity of gastric cancer stem cells, these cells were isolated from mice and cultured as gastric organoids (Figure 5A,E,I). At 24 weeks, organoid diameters in the combined exposure group (*H. pylori* + NMU, 53.52 ± 12.33 μm) were significantly smaller compared to the single exposure groups (*H. pylori*, 74.23 ± 14.28 μm; NMU, 69.9 ± 18.79 μm; both, $p < 0.001$) (Figure 5B). By 36 weeks, the inhibitory effect was more pronounced, with the *H. pylori* + NMU group (48.70 ± 11.62 μm) exhibiting significantly smaller organoids compared to the *H. pylori* or NMU group alone ($p < 0.01$) (Figure 5F). At 44 weeks, treatment with the autophagy inhibitor CQ partially reversed this inhibition, with the *H. pylori* + NMU + CQ group (70.63 ± 14.66 μm) showing a recovery in diameter, approaching that of the single CQ-treated groups. Moreover, the *H. pylori* + CQ group (93.74 ± 18.22 μm) exhibited the largest diameters among all CQ-treated conditions (Figure 5J).

Organoid numbers followed a similar trend of modulation across exposure groups (Figure 5C,G,K). At 24 weeks, the *H. pylori* group (66.00 ± 4.32) exhibited significantly higher organoid numbers compared with the control group (34.33 ± 4.03; $p < 0.001$), while NMU also increased organoid numbers (50.67 ± 2.49). In contrast, the *H. pylori* + NMU group (64.67 ± 3.40) showed no significant difference from the *H. pylori* group alone. At 36 weeks, organoid numbers in the *H. pylori* + NMU group (47.67 ± 2.05) were significantly lower than in the *H. pylori* group (61.33 ± 2.49; $p < 0.001$), highlighting a potential inhibitory interaction between *H. pylori* and NMU. By 44 weeks, CQ treatment elicited distinct effects, with the *H. pylori* + CQ group (58.00 ± 1.63) exhibiting the highest organoid numbers after treatment. In contrast, the NMU + CQ group (28.00 ±

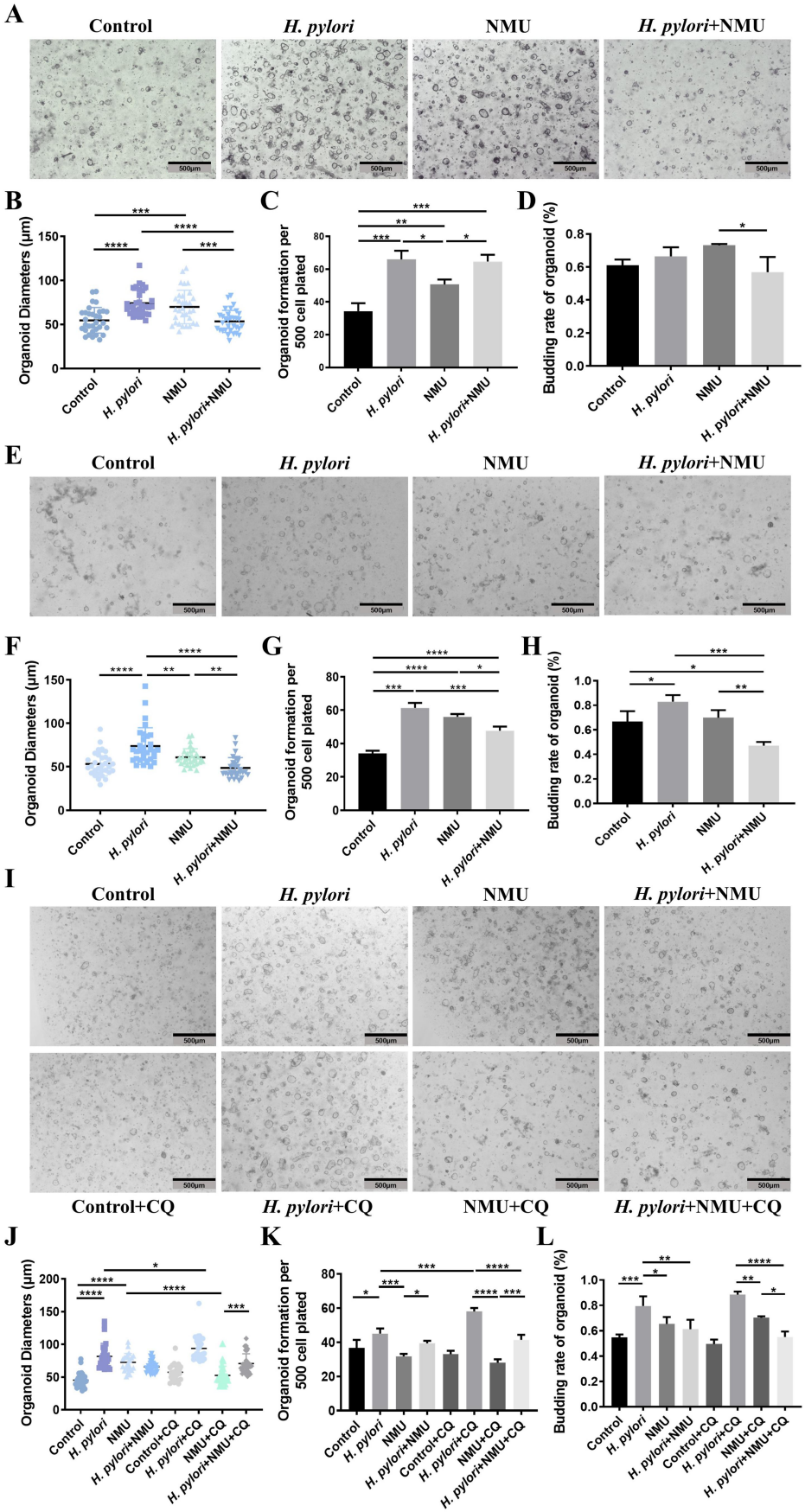

Figure 5. Gastric organoid growth and budding dynamics following *H. pylori*, N-nitroso-N-methylurea (NMU), and chloroquine exposure. (A, E, I) Representative images of gastric organoids at 24, 36, and 44 weeks. Scale bar: 500 μm. (B, F, J) comparisons of organoid diameters across experimental groups. (C, G, K) organoid number comparisons across different conditions. (D, H, L) budding analysis of gastric organoids under various treatments. The number of organoids is the total number of organoids in a single well of 24-well cell culture plate ($n = 6$). Statistical significance: *$p < 0.05$, **$p < 0.01$, ***$p < 0.001$, ****$p < 0.0001$.

1.63) showed a further decline in organoid numbers, and the *H. pylori* + NMU + CQ group (41.33 ± 2.49) showed only a slight increase compared with the *H. pylori* + NMU group without CQ.

Organoid budding varied across groups and time points (Figure 5D,H,L). At 24 weeks, the *H. pylori* + NMU group (0.57 ± 0.07% budding) showed a notable reduction, when compared with the NMU group (0.73 ± 0.01%). By 36 weeks, the *H. pylori* group (0.83 ± 0.04%) maintained the highest budding percent, while the *H. pylori* + NMU group showed a significant decline (0.47 ± 0.02%; $p < 0.01$) compared with NMU treatments. At 44 weeks, the *H. pylori* + NMU group showed reduced budding (0.61 ± 0.06%), which was significantly lower than either single exposure group (all, $p < 0.05$). CQ treatment further influenced budding. The *H. pylori* + CQ group had the highest budding (0.88 ± 0.02%; $p < 0.001$), while the NMU + CQ group (0.70 ± 0.01%) displayed a slight but significant increase over NMU alone ($p < 0.05$). However, the *H. pylori* + NMU + CQ group (0.55 ± 0.04%) showed no improvement compared with the *H. pylori* + NMU group.

H. pylori and NMU modulate gastric stem cell markers through CQ-sensitive pathways

To determine the expressions of gastric stem cell markers, qRT-PCR was performed to evaluate mRNA levels of *CD133*, *CD44*, *Lgr5*, and *SOX2* in mice at different ages (Figure 5).

At 24 weeks, the mRNA expression levels of *CD44*, *CD133*, *Lgr5*, and *SOX2* showed distinct changes in the experimental groups (Figure 6A). Compared to the control group, *H. pylori* treatment significantly increased the expression levels of *CD44*, *Lgr5*, and *SOX2* by approximately 35%, 92%, and 81%, respectively (all, $p < 0.05$), while the expression of *CD133* showed no significant difference. NMU treatment alone significantly decreased expression levels of *CD44* and *CD133* by 35% and 30%, respectively, while *Lgr5* levels increased by 85% (all, $p < 0.05$). The combined treatment of *H. pylori* + NMU exhibited unique expression patterns. Compared to the NMU group, the *CD44* and *CD133* levels significantly increased, while *SOX2* expression was significantly reduced, when compared with the *H. pylori* group (all, $p < 0.05$). Together, these results indicated that combined *H. pylori* + NMU treatment modulated mRNA expression differently, enhancing the levels of *CD44* and *CD133* relative to NMU treatment alone, while suppressing *SOX2*, compared with *H. pylori* treatment alone.

At 36 weeks, the mRNA expression levels of *CD44*, *CD133*, *Lgr5*, and *SOX2* exhibited notable changes in the experimental groups (Figure 6B). Both *H. pylori* and NMU treatments alone significantly increased the mRNA levels of these molecules, when compared with the Control group (all, $p < 0.05$), with the exception of

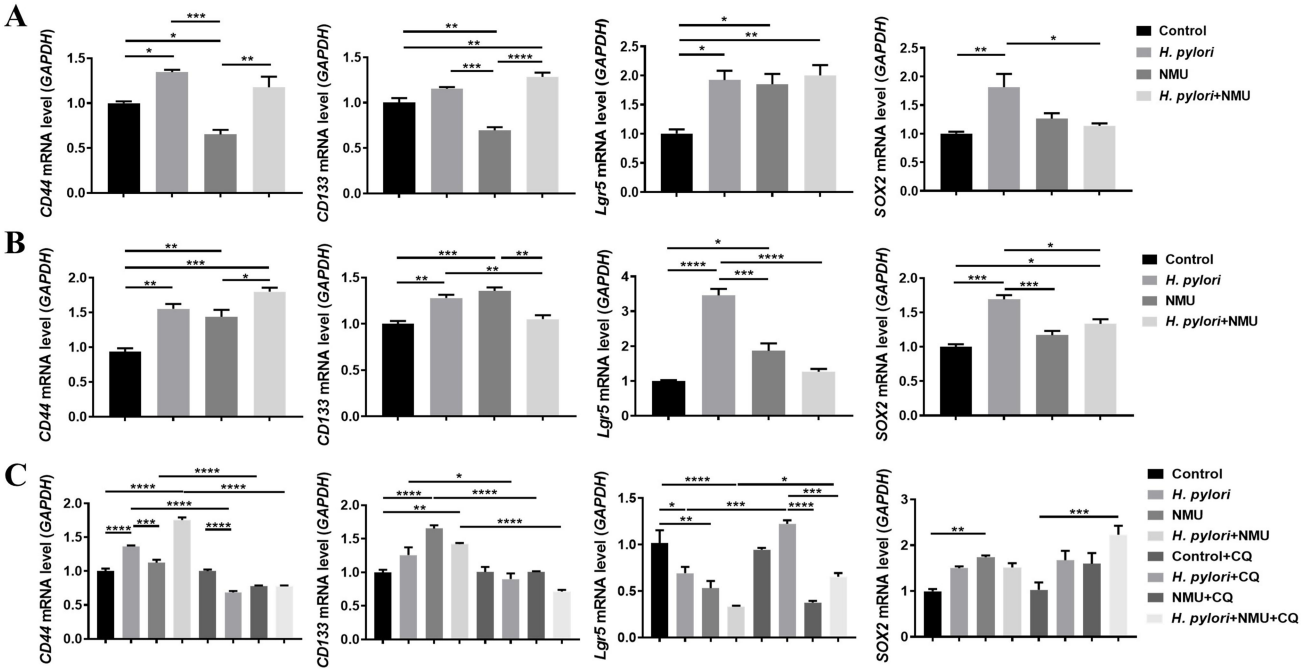

Figure 6. Expression of gastric stem cell markers in mice following *H. pylori*, N-nitroso-N-methylurea, and chloroquine exposure. expression level of *CD44*, *CD133*, *Lgr5*, and *SOX2* at (A) 24, (B) 36, and (C) 44 weeks of mice in each group was detected by qPCR ($n = 3$). Statistical significance: *$p < 0.05$, **$p < 0.01$, ***$p < 0.001$, ****$p < 0.0001$.

SOX2, which showed no significant change after NMU exposure. Specifically, the mRNA levels of *CD44* and *Lgr5* in the *H. pylori* group increased by approximately 65% and 246%, respectively, while NMU exposure elevated levels of *CD44* and *Lgr5* by 44% and 86%, respectively. *SOX2* levels increased significantly ($p < 0.05$) in the *H. pylori* group by 69%. In the combined *H. pylori* + NMU treatment group, distinct trends were observed. The mRNA levels of *CD133*, *Lgr5*, and *SOX2* were significantly reduced compared with the *H. pylori* group alone (all, $p < 0.05$), indicating a suppressive effect of combined exposure. Notably, *CD44* expression in the combined group was significantly higher than in the NMU group ($p < 0.05$), whereas *CD133* expression was significantly lower ($p < 0.01$), when compared with NMU alone. Together, these results showed that combined exposure to *H. pylori* and NMU modulated mRNA expression of these molecules differently than individual treatments, suggesting potential interactions between these treatments during alterations of gene expressions.

At 44 weeks, mRNA expression levels of *CD44*, *CD133*, *Lgr5*, and *SOX2* showed significant variations in different treatment groups (Figure 6C). Exposure to *H. pylori* alone increased *CD44* expression by 37% compared with the control group, while *Lgr5* levels were reduced by approximately 32% (both, $p < 0.05$). When CQ was administered with *H. pylori*, *CD44* levels decreased by 49%, and *Lgr5* levels increased by 77%, indicating a notable reversal of the effects induced by *H. pylori* alone. In the NMU-treated group, *CD133* and *SOX2* levels rose by 65% and 74%, respectively, while *Lgr5* levels were reduced by nearly 48% compared with the control (all, $p < 0.01$). The addition of CQ to NMU-treated groups caused *CD133* expression to decrease ($p < 0.0001$) by approximately 57%, showing a pronounced inhibitory effect. For the combined *H. pylori* + NMU exposure group, the addition of CQ resulted in significant changes. *CD44* and *CD133* levels decreased by 55% and 50% (both, $p < 0.0001$), respectively, relative to the *H. pylori* + NMU group without CQ, while *Lgr5* and *SOX2* levels rose by 97% and 47%, respectively (both, $p < 0.05$). Taken together, these findings suggested that CQ modulated mRNA expression patterns induced by *H. pylori* and NMU, and also had variable effects on different molecules, either amplifying or attenuating their expression changes.

Autophagy inhibition by CQ reduces H. pylori- and NMU-induced gastric pathology

At 24 weeks of age, H&E staining revealed that the control group had a normal gastric structure with no inflammatory cell infiltration. In contrast, the NMU group showed clear inflammatory infiltration at the base of the mucosal layer, while the *H. pylori* + NMU group exhibited mild structural abnormalities, including dilation of gastric pits and fundic glands, with significant neutrophil infiltration in the submucosa (Figure 7A). At 36 weeks, the Control group maintained a normal gastric structure without inflammation. However, the *H. pylori* group showed gastric mucosal atrophy, glandular expansion, and inflammatory infiltration. The NMU group displayed more pronounced inflammation, while the *H. pylori* + NMU group showed abnormal gastric structure, with glandular dilation, intestinal metaplasia, and heavy neutrophil infiltration (Figure 7B). By 44 weeks, the *H. pylori* group demonstrated moderate gastric atrophy, epithelial exfoliation, and increased inflammatory infiltration. In the NMU group, severe glandular abnormalities and inflammation were observed. The *H. pylori* + NMU group had extensive glandular expansion, intestinal metaplasia, and heavy neutrophil infiltration. After CQ treatment, both the *H. pylori* + CQ and *H. pylori* + NMU + CQ groups showed reduced inflammation and glandular dilation, with necrotic areas appearing in the *H. pylori* + NMU + CQ group (Figure 7C).

Discussion

Autophagy modulates the host response to chronic *H. pylori* infection, with the bacteria inducing autophagy in gastric epithelial cells. This occurs through mechanisms like VacA-mediated incomplete autophagosome formation and Beclin1-Vps34-dependent activation, promoting both host defense and bacterial persistence [11,30–34]. Our study showed that *H. pylori* and NMU co-exposure upregulated LC3B expression and increased autophagic structures, particularly in the *H. pylori* + NMU group, indicating NMU amplifies autophagy to sustain infection (Figure 1, 2). Chloroquine (CQ), an autophagy inhibitor, mitigated these effects by blocking autophagic degradation and reducing *H. pylori* virulence, as evidenced by LC3B accumulation. These findings align with clinical observations of LC3 overexpression in 58% of human gastric cancers, where elevated LC3 levels correlate with advanced stage and poor prognosis [35,36]. The clinical potential of autophagy inhibition is further supported by Phase I/II trials demonstrating good tolerance and efficacy of CQ derivatives in combination therapies for various cancers [37]. These results provide a strong rationale for exploring CQ-based autophagy-targeted therapies in *H. pylori*-related gastric diseases, particularly for

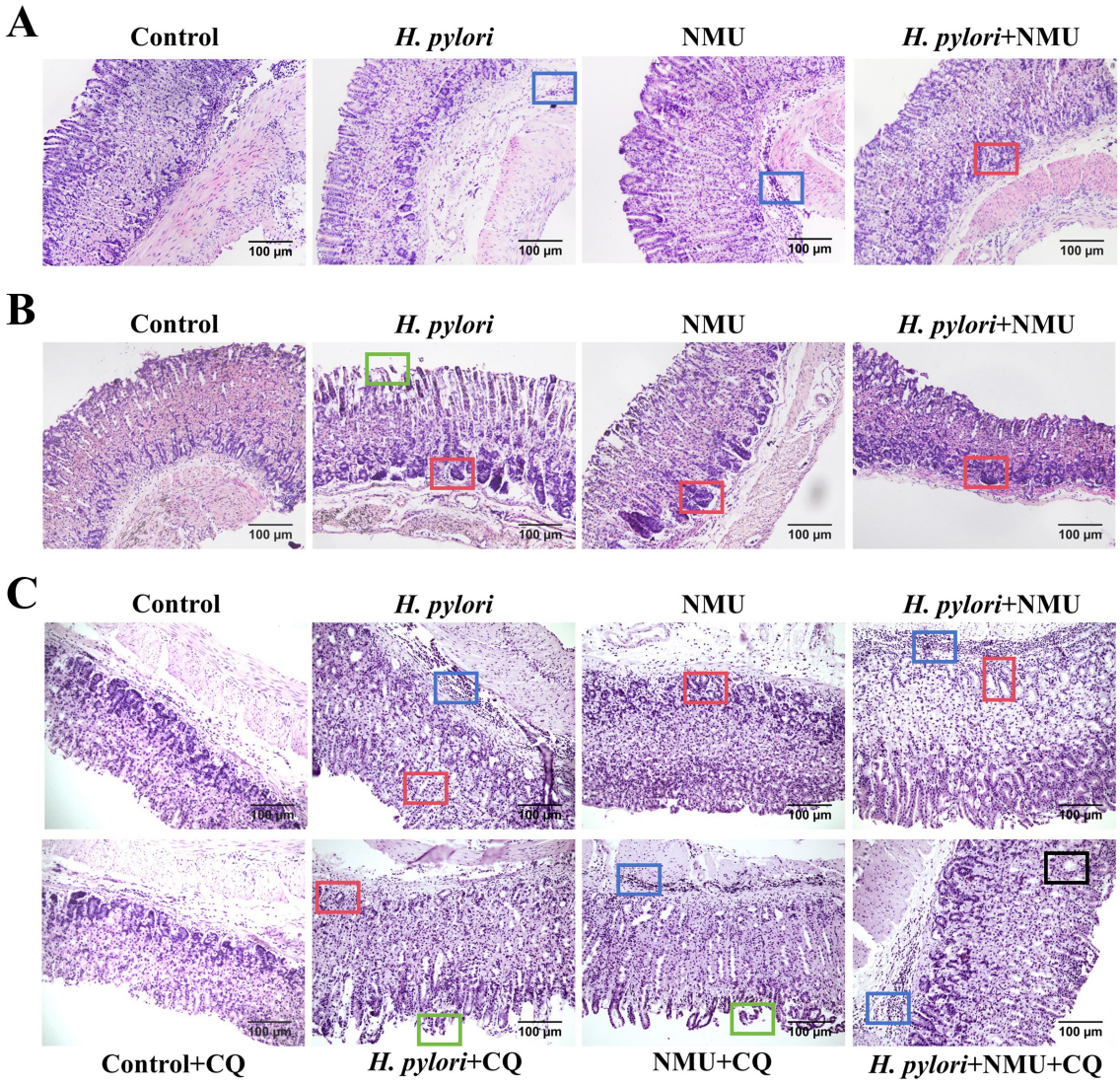

Figure 7. Histopathological changes in gastric tissues of mice under *H. pylori*, N-nitroso-N-methylurea, and chloroquine exposure. histopathological changes were observed at (A) 24 weeks, (B) 36 weeks, and (C) 44 weeks. Inflammatory cell infiltration (blue), glandular swelling and expansion (red), intestinal metaplasia (orange), glandular shedding (green), and tissue necrosis (black) are indicated by their respective rectangles ($n = 6$). Scale bar: 100 μm.

treatment-resistant infections or high-risk patients with precancerous lesions.

The EMT is a critical process in tumor progression, particularly in the migration and invasion of cancer cells [38]. Our study demonstrated that *H. pylori* infection and NMU exposure significantly enhanced the EMT in gastric tissue, as indicated by the decreased expression of E-cadherin, reflecting a stronger shift from epithelial to mesenchymal cells (Figure 3). This EMT induction suggests pathological stem cell differentiation, contributing to tumor progression and disrupted tissue homeostasis [39,40]. Our data reveal that *H. pylori* infection disrupts gastric homeostasis by coordinately suppressing *Ghrelin* and *E-cadherin* while later inducing *Tff2*—a pattern exacerbated by NMU co-treatment (Figure 4). The *Ghrelin* downregulation likely impairs AMPK-mediated autophagy and activates mTOR [15], promoting the EMT through Snail/Twist upregulation and E-cadherin degradation [41]. Conversely, the sustained *Tff2* overexpression – potentiated by *H. pylori* + NMU – may drive β-catenin nuclear translocation, as evidenced in pancreatic models, where TFF2/β-catenin complexes upregulate EMT effectors and inhibit apoptosis [42]. CQ's differential effects (rescuing *E-cadherin* but amplifying *Tff2*) suggest autophagy inhibition preferentially blocks the Ghrelin-AMPK-EMT axis while permitting β-catenin-mediated Tff2 signaling. This duality underscores a crosstalk between Ghrelin-autophagy and Tff2/β-catenin pathways in *H. pylori*-induced EMT, where

Ghrelin loss exacerbates mucosal injury while Tff2 elevation may facilitate pre-neoplastic plasticity. Clinically, EMT drives invasiveness and drug resistance in *H. pylori*-related gastric cancer, as seen in pazopanib-treated xenografts with upregulated cancer stem cell markers

. Targeting the EMT with autophagy inhibitors may reduce tumor progression and overcome resistance.

H. pylori infection promotes gastric cancer via chronic inflammation, genotoxic stress, and gastric stem cell dysregulation [43]. It also enhances epithelial proliferation and synergizes with carcinogens to drive aberrant stem cell behavior [44,45]. In this study, *H. pylori* significantly increased organoid size, number, and budding, with peak effects at 36 weeks (Figure 5). This persistent stem cell activation underscores the role of *H. pylori* as an early carcinogenic driver. Combined *H. pylori* and NMU exposure initially showed synergistic effects, but over time, resulted in suppression of organoid size, number, and budding, particularly by 44 weeks (Figure 5). This suppression likely results from synergistic inflammation and genotoxicity, collectively disrupting stem cell homeostasis and accelerating gastric pathology [46]. These findings suggest that combined exposure altered stem cell behavior and also expedited the progression of precancerous lesions to malignancy. Autophagy, with protective and tumor-promoting roles in gastric stem cell regulation [47], enhances *H. pylori*-induced Wnt/β-catenin signaling and organoid growth [48]. However, in the *H. pylori* + NMU co-exposure model, CQ only partially alleviated suppression and failed to restore organoid morphology, suggesting that the combined inflammatory and genotoxic stress overwhelms the protective capacity of autophagy. These findings highlight the need for therapeutic strategies that simultaneously target both pathogenic pathways in gastric carcinogenesis.

Bacterial infections and carcinogens can drive cancer progression by disrupting stem cell function [49]. Our study showed that *H. pylori* and NMU significantly altered gastric stem cell markers, impacting stem cell regulation (Figure 6). *H. pylori* infection increased *CD44* and *Lgr5* expression, which are linked to stem cell self-renewal and gastric gland regeneration, respectively, consistent with its role in promoting stem cell proliferation during chronic inflammation [50,51] and creating a carcinogenic microenvironment [52]. NMU initially upregulated *Lgr5*, likely for tissue repair, but later suppressed differentiation markers like *SOX2*, reflecting its genotoxic effect on the stem cell niche [45]. Combined *H. pylori* and NMU exposure intensified these effects, elevating *CD44* and *CD133* while reducing *Lgr5*, indicating disrupted stem cell dynamics. CQ treatment mitigated these changes by reducing *CD44* and *CD133*, while restoring *Lgr5* and *SOX2* expression, promoting epithelial differentiation and normal stem cell function, consistent with autophagy inhibition reducing pathological proliferation [53,54]. These findings highlight the role of autophagy in mediating *H. pylori*- and NMU-driven stem cell changes, suggesting a therapeutic approach to counter inflammation-driven carcinogenesis.

Previous studies have reported that autophagy inhibition by CQ regulates necrosis and promotes tissue repair in various cell types and during bacterial infections [55]. *H. pylori* infection and NMU exposure caused significant gastric tissue damage, including inflammation, glandular dilation, and disruption. Combined exposure intensified these effects, leading to intestinal metaplasia and increased neutrophil infiltration, indicating a synergistic role in gastric injury. CQ, an autophagy inhibitor, reduced inflammation and glandular dilation in both *H. pylori* and *H. pylori* + NMU groups, suggesting autophagy drives damage from chronic infection and carcinogen exposure (Figure 7). CQ inhibited autophagic degradation, reducing uncontrolled autophagy, inflammation, and promoting tissue recovery [56]. By shifting cellular responses from excessive autophagy to controlled necrosis, CQ facilitated damaged cell clearance, reduced neutrophil infiltration, and restored gastric gland structure [57,58]. This suggests the potential of CQ as a therapeutic agent for managing *H. pylori*-induced gastric damage, especially with carcinogenic co-exposure.

This study has two key limitations that warrant further investigation. First, while mouse models provide mechanistic insights, they may not fully replicate human *H. pylori* pathogenesis, requiring cautious clinical translation and phase I trials to assess long-term CQ safety (including gastrointestinal and microbiome effects). Additionally, although our 24–44 weeks of observation captured early pathology, longer durations are needed to monitor progression to advanced pre-neoplastic stages. Future studies should therefore: (1) establish longer-term preclinical models to delineate the complete temporal dynamics of *H. pylori*- and NMU-driven carcinogenesis, and (2) systematically evaluate combined CQ with targeted anti-inflammatory/genotoxic therapies on stem cell regulation and disease progression.

Conclusion

This study systematically elucidated the critical role of autophagy regulation in the pathogenesis of *H. pylori*-associated gastric diseases. Our findings demonstrate that *H. pylori* infection disrupts gastric stem cell

homeostasis by activating autophagy pathways, leading to abnormal proliferation, self-renewal, and differentiation of stem cells. Co-exposure with the carcinogen NMU exacerbates this process through synergistic promotion of inflammatory responses and genotoxic stress, accelerating EMT and gastric mucosal pathological changes. Although CQ partially restored stem cell function and alleviated tissue damage by inhibiting autophagy, its limited efficacy in reversing severe pathological remodeling suggests the constraints of autophagy-targeted monotherapy. Based on these findings, we recommend the following future research focus: 1) development of more human-relevant mouse models with extended observation periods; and 2) exploration of combination therapies of autophagy inhibitors with anti-inflammatory or anti-genotoxic agents.

Acknowledgements

We thank International Science Editing (http://www.internationalscienceediting.com) for editing this manuscript.

Jing Li and Sisi Liu contributed equally as first authors, leading the original draft writing, data acquisition, and investigation. Zhiqin Li and Chunlei Ma contributed to the investigation and formal analysis. Yingzi Cui handled software implementation and methodology. Wenke Wang supported data curation. Huilin Zhao and Xiaofei Ji contributed to data acquisition and analysis. Boqing Li and Ying Zhang designed and supervised the study, provided resources, contributed to data interpretation, and managed project administration. All authors contributed to manuscript revisions and editing and approved the final manuscript.

Author contributions

CRediT: **Jing Li:** Data curation, Investigation, Writing – original draft; **Sisi Liu:** Data curation, Investigation, Writing – original draft; **Zhiqin Li:** Formal analysis, Investigation; **Chunlei Ma:** Formal analysis, Investigation; **Boqing Li:** Data curation, Project administration, Writing – review & editing; **Yingzi Cui:** Methodology, Software; **Wenke Wang:** Data curation; **Huilin Zhao:** Data curation, Formal analysis; **Xiaofei Ji:** Data curation, Formal analysis; **Ying Zhang:** Funding acquisition, Investigation, Project administration, Writing – review & editing.

Funding

This work was supported by the National Natural Science Foundation of China under Grant 82172560; the Taishan Scholar Foundation of Shandong Province, China under Grant tsqn202211229; special supporting funds for Leading Talents above the Provincial Level in Yantai city, China; and Yantai Science and Technology Development Project (2022JCYJ024).

Disclosure statement

No potential conflict of interest was reported by the author(s).

Data availability statement

The data generated during the study is available at https://doi.org/10.6084/m9.figshare.29579378.

ORCID

Huilin Zhao http://orcid.org/0009-0006-4449-354X
Ying Zhang http://orcid.org/0000-0002-4452-2359

References

[1] Correa P, Piazuelo MB. *Helicobacter pylori* infection and gastric adenocarcinoma. US Gastroenterol Hepatol Rev. 2011;7(1):59–64.
[2] Kusters JG, van Vliet AHM, Kuipers EJ. Pathogenesis of *helicobacter pylori* infection. Clin Microbiol Rev. 2006;19(3):449–490. doi: 10.1128/CMR.00054-05
[3] Sano T. Gastric cancer: asia and the world. Gastric Cancer. 2017;20(Suppl S1):1–2. doi: 10.1007/s10120-017-0694-9
[4] Tegtmeyer S, Backert N. *Helicobacter pylori* infection of AZ-521 cells reveals a type IV secretion defect and VacA-independent CagA phosphorylation. FEBS J. 2017;284(10):1428–1441. doi: 10.1242/dmm.032813
[5] Tegtmeyer N, Backert S, Rohde M. Role of the *Helicobacter pylori* cag-pathogenicity island in gastric border cell signaling and cytoskeleton reorganization. Gut Microbes. 2011;2(4):230–234.
[6] Loomis D, Huang W, Chen G. The International Agency for Research on Cancer (IARC) evaluation of the carcinogenicity of outdoor air pollution: focus on China. Chin J Cancer. 2014;33(4):189–196. doi: 10.5732/cjc.014.10028
[7] Wang F, Meng W, Wang B, et al. *Helicobacter pylori*-induced gastric inflammation and gastric cancer. Cancer Lett. 2014;345(2):196–202. doi: 10.1016/j.canlet.2013.08.016
[8] Wizenty J, Sigal M. Gastric stem cell biology and *Helicobacter pylori* infection: Curr Top Microbiol Immunol. 2023.doi:10.1007/978-3-031-47331-9_1
[9] Liu M, Liu Q, Zou Q, et al. The composition and roles of gastric stem cells in epithelial homeostasis, regeneration, and tumorigenesis. Cell Oncol. 2023;46(4):867–883. doi: 10.1007/s13402-023-00802-z
[10] Sbrana FV, Cortini M, Avnet S, et al. The role of autophagy in the maintenance of stemness and differentiation of mesenchymal stem cells. STEM Cell Rev And Rep. 2016;12(6):621–633. doi: 10.1007/s12015-016-9690-4
[11] Courtois S, Haykal M, Bodineau C, et al. Autophagy induced by *Helicobacter pylori* infection is necessary for gastric cancer stem cell emergence. Gastric Cancer. 2021;24(1):133–144. doi: 10.1007/s10120-020-01118-9
[12] Ding SZ, Zheng PY. *Helicobacter pylori* infection induced gastric cancer; advance in gastric stem cell

research and the remaining challenges. Gut Pathog. 2012;4(1):18. doi: 10.1186/1757-4749-4-18
[13] Marcucci F, Ghezzi P, Rumio C. The role of autophagy in the cross-talk between epithelial-mesenchymal transitioned tumor cells and cancer stem-like cells. Mol Cancer. 2017;16(3). doi: 10.1186/s12943-016-0573-8
[14] Pradella D, Naro C, Sette C, et al. Emt and stemness: flexible processes tuned by alternative splicing in development and cancer progression. Mol Cancer. 2017;16(8). doi: 10.1186/s12943-016-0579-2
[15] Babaei G, gholizadeh-Ghaleh Aziz S, Zare Zavieyh Jaghi N. Emt, cancer stem cells and autophagy: the three main axes of metastasis. Biomed Pharmacother. 2021;133:110909. doi: 10.1016/j.biopha.2020.110909
[16] Jason S, Cui W. Proliferation, survival and metabolism: the role of PI3K/AKT/mTOR signalling in pluripotency and cell fate determination. Development. 2016;143(17):3050–3060. doi: 10.1242/dev.137075
[17] Chen HT, Liu H, Mao MJ, et al. Crosstalk between autophagy and epithelial-mesenchymal transition and its application in cancer therapy. Mol Cancer. 2019;18(1):101. doi: 10.1186/s12943-019-1030-2
[18] Hao Y, Baker D, ten Dijke P. TGF-β-mediated epithelial-mesenchymal transition and cancer metastasis. Int J Mol Sci. 2019;20(11):2767. doi: 10.3390/ijms20112767
[19] Serrano-Gomez SJ, Maziveyi M, Alahari SK. Regulation of epithelial-mesenchymal transition through epigenetic and post-translational modifications. Mol Cancer. 2016;15(1):18. doi: 10.1186/s12943-016-0502-x
[20] Wang S, Guo H, Jia J, et al. Silencing TAB182 inhibits cell EMT, migration and invasion by downregulating EGFR in A549 NSCLC cells. Mol Biol Rep. 2023;50(4):3073–3083. doi: 10.1007/s11033-022-08176-5
[21] Rossi G, Manfrin A, Lutolf MP. Progress and potential in organoid research. Nat Rev Genet. 2018;19(11):671–687. doi: 10.1038/s41576-018-0051-9
[22] Sato T, Vries RG, Snippert HJ, et al. Single *lgr5* stem cells build crypt-villus structures in vitro without a mesenchymal niche. Nature. 2009;459(7244):262–265. doi: 10.1038/nature07935
[23] Clevers H. Modeling development and disease with organoids. Cell. 2016;165(7):1586–1597. doi: 10.1016/j.cell.2016.05.082
[24] Lancaster MA, Knoblich JA. Organogenesis in a dish: modeling development and disease using organoid technologies. Science. 2014;345(6194):1247125. doi: 10.1126/science.1247125
[25] Sato T, Clevers H. Growing self-organizing mini-guts from a single intestinal stem cell: mechanism and applications. Science. 2013;340(6137):1190–1194. doi: 10.1126/science.1234852
[26] Burkitt MD, Duckworth CA, Williams JM, et al. *Helicobacter pylori*-induced gastric pathology: insights from in vivo and ex vivo models. Disease Model Mechanisms. 2017;10(2):89–104. doi: 10.1242/dmm.027649
[27] Qadri Q, Rasool R, Gulzar GM, et al. *H. pylori* infection, inflammation and gastric cancer. J Gastrointest canc. 2014;45(2):126–132. doi: 10.1007/s12029-014-9583-1
[28] Diab KAS, Aboul-Ela EI. In vivo comparative studies on antigenotoxicity of date palm (Phoenix dactylifera L.) pits extract against DNA damage induced by N-nitroso-N-methylurea in mice. Toxicol Int. 2012;19(3):279–286. doi: 10.4103/0971-6580.103669
[29] Li B, He J, Zhang R, et al. Integrin-linked kinase in the development of gastric tumors induced by *Helicobacter pylori*: regulation and prevention potential. Helicobacter. 2024;29(4):e13109. doi: 10.1111/hel.13109
[30] Akbari A, Noorbakhsh Varnosfaderani SM, Haeri MS, et al. Autophagy induced by *Helicobacter pylori* infection can lead to gastric cancer dormancy, metastasis, and recurrence: new insights. Hum Cell. 2024;37(1):139–153. doi: 10.1007/s13577-023-00996-2
[31] Chu H, et al. *Helicobacter pylori* and autophagy: a new facet in cellular defense against bacterial infection. Autophagy. 2010;6(1):123–124.
[32] Terebiznik MR, Vazquez CL, Torbicki K, et al. Helicobacter pylori VacA toxin promotes bacterial intracellular survival in gastric epithelial cells. J Cell Biol. 2009;188(3):425–436.
[33] Zhang F, Chen C, Hu J, et al. Molecular mechanism of *helicobacter pylori*-induced autophagy in gastric cancer: a review. Oncol Lett. 2019;18(6):6221–6227. doi: 10.3892/ol.2019.10976
[34] Zhu P, Xue J, Zhang Z, et al. *Helicobacter pylori* vacA induces autophagic cell death in gastric epithelial cells via the endoplasmic reticulum stress pathway. Cell Death Dis. 2017;8(12):3207. doi: 10.1038/s41419-017-0011-x
[35] Liao W, Sun L, Wang C, et al. LC3A-positive "stone-like" structures predict an adverse prognosis of gastric cancer. Anatomical record. 2014;297(4):653–662. doi: 10.1002/ar.22895
[36] Yoshioka A, Miyata H, Doki Y, et al. LC3, an autophagosome marker, is highly expressed in gastrointestinal cancers. Int J Oncol. 2008;33:461–468.
[37] Amaravadi RK, Kimmelman AC, Debnath J. Targeting autophagy in cancer: recent advances and future directions. Cancer Discov. 2019;9(9):1167–1181. doi: 10.1158/2159-8290.CD-19-0292
[38] Huang Y, Hong W, Wei X. The molecular mechanisms and therapeutic strategies of EMT in tumor progression and metastasis. J Hematol Oncol. 2022;15(1):129. doi: 10.1186/s13045-022-01347-8
[39] Den Hollander P, Maddela JJ, Mani SA. Spatial and temporal relationship between epithelial–mesenchymal transition (EMT) and stem cells in cancer. Clin Chem. 2024;70(1):190–205. doi: 10.1093/clinchem/hvad197
[40] Lambert AW, Weinberg RA. Linking EMT programmes to normal and neoplastic epithelial stem cells. Nat Rev Cancer. 2021;21(5):325–338. doi: 10.1038/s41568-021-00332-6
[41] Roshan MK, Soltani A, Soleimani A, et al. Role of AKT and mTOR signaling pathways in the induction of epithelial-mesenchymal transition (EMT) process. Biochimie. 2019;159:56–64.
[42] Zhou Y, Zhang Y, Wang J. Trefoil factor 2 regulates proliferation and apoptosis of pancreatic cancer cells and LPS-induced normal pancreatic duct cells by β-catenin pathway. Cancer Manag Res, 12, 10705–10713 (2020). doi: 10.2147/CMAR.S274578
[43] Graham DY, Lu H, Yamaoka Y. *Helicobacter pylori* pathogenesis and stem cell modulation. Gastroenterology. 2014;147:32–42.

[44] Sayi A, Chen Y, Zhou Z. *Helicobacter pylori* and its effect on Wnt/β-catenin signaling in gastric cancer. J Clin investigation. 2011;121:844–853.
[45] Shibata W, Takaishi S, Muthupalani S. Genotoxic stress in NMU-induced gastric changes. Cancer Res. 2016;76:3531–3542.
[46] Wroblewski LE, Peek RM, Wilson KT. *Helicobacter pylori* and epithelial-mesenchymal signaling in gastric carcinogenesis. Gastroenterology. 2010;138:819–831.
[47] Deretic V, Saitoh T, Akira S. Autophagy in infection, inflammation, and immunity. Nat Rev Immunol. 2013;13(10):722–737. doi: 10.1038/nri3532
[48] Xu Y, Eom T, Nam S. Role of autophagy inhibition in stem cell signaling. Cell Rep. 2019;26:1104–1112.
[49] Barker N, van Es JH, Kuipers J, et al. Identification of stem cells in small intestine and colon by marker gene *Lgr5*. Nature. 2010;449(7165):1003–1007. doi: 10.1038/nature06196
[50] Sigal M, Rothenberg ME, Logan CY, et al. *Helicobacter pylori* activates and expands *Lgr5*(+) stem cells through direct colonization of the gastric glands. Gastroenterology. 2015;148(7):1392–1404.e21. doi: 10.1053/j.gastro.2015.02.049
[51] Walter RJ, Sonnentag SJ, Munoz-Sagredo L, et al. Wnt signaling is boosted during intestinal regeneration by a *CD44*-positive feedback loop. Cell Death Disease. 2022;13(2):168. doi: 10.1038/s41419-022-04607-0
[52] Misra SR, Marrogi A, Cram EJ, et al. *CD44* and its role in gastric cancer stem cell maintenance and tumorigenesis. Clin Cancer Res. 2015;21:3232–3240.
[53] Boya P, González-Polo RA, Casares N, et al. Inhibition of autophagy can preserve epithelial structure by preventing apoptosis. Mol Cell Biol. 2005;25(3):1029–1040. doi: 10.1128/MCB.25.3.1025-1040.2005
[54] Maycotte P, Jones KL, Goodall ML, et al. Autophagy supports breast cancer stem cell maintenance by regulating IL6 secretion. Mol Cancer Res. 2015;13(4):651–658. doi: 10.1158/1541-7786.MCR-14-0487
[55] Yu Z, Zhao Y, Ding K, et al. Chloroquine inhibition of autophagy enhanced the anticancer effects of *listeria monocytogenes* in melanoma. Microorganisms. 2023;11(2):408. doi: 10.3390/microorganisms11020408
[56] Cocco S, Leone A, Roca MS, et al. Inhibition of autophagy by chloroquine prevents resistance to PI3K/AKT inhibitors and potentiates their antitumor effect in combination with paclitaxel in triple negative breast cancer models. J Transl Med. 2022;20(1):290. doi: 10.1186/s12967-022-03462-z
[57] Thein W, Po WW, Choi WS, et al. Autophagy and digestive disorders: advances in understanding and therapeutic approaches. Biomol Ther (seoul). 2021;29(4):353–364. doi: 10.4062/biomolther.2021.086
[58] Yu Q, Ding J, Li S, et al. Autophagy in cancer immunotherapy: perspective on immune evasion and cell death interactions. Cancer Lett. 2024;590:216856. doi: 10.1016/j.canlet.2024.216856